

## Optically active erbium centers in silicon

H. Przybylinska

*Institut für Experimentalphysik, Johannes-Kepler-Universität, A-4040 Linz-Auhof, Austria  
and Institute of Physics, Polish Academy of Sciences, PL-02 668 Warsaw, Poland*

W. Jantsch

*Institut für Experimentalphysik, Johannes-Kepler-Universität, A-4040 Linz-Auhof, Austria*

Yu. Suprun-Belevitch

*Institut für Experimentalphysik, Johannes-Kepler-Universität, A-4040 Linz-Auhof, Austria  
and Belarussian State University, 220050 Minsk, Belarus*

M. Stepikhova

*Institut für Experimentalphysik, Johannes-Kepler-Universität, A-4040 Linz-Auhof, Austria  
and State University, 603600 Nizhny Novgorod, Russia*

L. Palmethofer and G. Hendorfer

*Institut für Experimentalphysik, Johannes-Kepler-Universität, A-4040 Linz-Auhof, Austria*

A. Kozanecki

*Institute of Physics, Polish Academy of Sciences, PL-02 668 Warsaw, Poland  
and Department of Electronic and Electrical Engineering, University of Surrey, Guildford, Surrey GU2 5XH, United Kingdom*

R. J. Wilson and B. J. Sealy

*Department of Electronic and Electrical Engineering, University of Surrey, Guildford, Surrey GU2 5XH, United Kingdom*

(Received 25 January 1996; revised manuscript received 28 March 1996)

The intra- $4f$  transition close to  $1.54\ \mu\text{m}$  of Er implanted into Si shows rich fine structure due to the crystal field of different defect types. Making use of the influence of implantation and annealing parameters, additional doping, temperature, and excitation power, we identify groups of lines belonging to different Er-related, optically active defects: the isolated interstitial Er, axial symmetry Er complexes with oxygen, and Er complex centers containing residual radiation defects. We show that the exciton binding energies as well as nonradiative quenching rates differ for different Er centers. Under optimum annealing conditions, the isolated interstitial Er has the highest photoluminescence yield at temperatures above 100 K. [S0163-1829(96)03327-9]

### I. INTRODUCTION

The enormous progress achieved in the last decade in the development of fiber optics communication systems has stimulated growing interest in temperature-stable light sources emitting at wavelengths of about  $1.5\ \mu\text{m}$ , i.e., the wavelength corresponding to minimum loss and low dispersion of silica-based optical fibers. One possible candidate for a temperature-stable emission at this wavelength is erbium as an impurity in various semiconductors, since the internal transition between the two lowest spin-orbit levels of  $\text{Er}^{3+}$ , namely,  ${}^4I_{13/2} \rightarrow {}^4I_{15/2}$ , occurs at approximately  $1.54\ \mu\text{m}$ .<sup>1</sup> Due to the closed  $5s^2 5p^6$  outer shells, which screen very effectively the unfilled  $4f^{11}$  shell, the interaction of the Er ion with the host matrix is weak and the wavelength of the intra- $4f$ -shell emission depends little on the actual host and is practically temperature independent. In the later respect, erbium-doped systems appear attractive as compared to near-band-edge lasers based on III-V compounds, which suffer from the relatively large temperature coefficients of their energy gaps. Another characteristic feature of the above-

mentioned intra- $4f$  transitions is their low transition probability, which makes the excited-state lifetimes long enough to achieve population inversion easily. This inversion is successfully utilized in erbium-doped optical fibers, where stimulated emission after optical pumping into higher excited  $4f$  states is used for in-fiber optical amplification of the  $1.54\ \mu\text{m}$  signal.

Among the various erbium-doped semiconductor systems, Si:Er appears to be particularly attractive since the advanced processing technology of silicon offers great application possibilities, not only for integrated fiber optics sources but also for optical data transfer within and between large-scale integrated circuits. It is thus not surprising that the optical activity of Er in Si has received a lot of attention recently.<sup>1-16</sup> However, owing to the weak coupling of Er atoms and the Si-host crystal, the low solubility, and the long radiative lifetime, the luminescence yield is only moderate at low temperatures and rather prohibitive for device applications at room temperature. Its improvement requires a detailed understanding of all processes limiting the erbium incorporation as well as the excitation and deexcitation efficiencies.

Extensive studies of Er implanted into Si have shown that the optical yield depends drastically on the material used, and it is typically one to two orders of magnitude higher in Czochralski-grown (CZ) Si as compared to the ultrapure float-zone (FZ) material.<sup>4–6</sup> This improvement is usually believed to be related to Er interacting with oxygen,<sup>4,7–11</sup> which is contained in CZ Si in concentrations of the order of  $10^{18}$   $\text{cm}^{-3}$ , already above the solubility limit of Er in Si.<sup>12</sup> It has also been found that the luminescence intensity increases substantially, especially in FS Si, with coimplantation of light elements, such as C, N, O, or F.<sup>4,5</sup> The additional ligand field introduced by the impurity is again held responsible for the observed enhancement.<sup>4,5</sup> Still, the number of optically active Er centers is estimated to be much lower than the number of incorporated Er ions.<sup>10</sup> Nevertheless, room-temperature Er photoluminescence (PL) and electroluminescence (EL) were recently achieved in CZ Si coinplanted with oxygen.<sup>9,10,13</sup>

The identification of the microscopic structure of the optically active Er centers and their preparation conditions therefore seem to be crucial for optimizing the erbium emission. Most of the usual methods that yield microscopic information on the defect structure may prove the existence of a particular defect but they do not allow direct, unequivocal identification of those defects which produce strong PL. In particular, in EPR, which is the most powerful method to investigate the microscopic structure of defects in solids, an  $\text{Er}^{3+}$  signal corresponding to a  $\Gamma_8$  state has been observed only under sample illumination. The parameters of such a state indicate that the center would have an entirely different emission spectrum than the one dominating the PL.<sup>14</sup>

In this paper, we present a study of Er-implanted Si by means of high-resolution Fourier PL spectroscopy as well as by deep-level transient spectroscopy (DLTS). We find more than 100 narrow PL lines in the region of 1.53–1.54  $\mu\text{m}$ . Some of these lines are split by only a fraction of a wave number but show completely different temperature and excitation dependence. The possibility of investigating the influence of temperature and excitation power density, as well as implantation and annealing parameters, on each of the emission lines separately enables us to identify the PL spectra of an isolated Er ion as well as two oxygen-related centers of nearly axial site symmetry. In addition, we find three other groups of lines, related to Er complexes with residual radiation defects, which we are able to classify according to their similar behavior with respect to the variation of parameters. We infer also that the dominant PL excitation mechanism in Si:Er involves defect Auger recombination of excitons bound on Er centers or Er-defect complexes, with binding energies varying for different centers. Moreover, the various Er centers also exhibit different quenching behavior at high temperatures. We show, in particular, that in well-annealed samples the emission of isolated Er centers dominates in the high-temperature PL. Finally, we discuss the beneficial effects of O codoping in terms of passivation of other recombination channels.

## II. EXPERIMENT

The samples used for PL investigations were (100)-oriented,  $n$ -type (phosphorus-doped) and  $p$ -type (boron-

doped) CZ and FZ silicon wafers, with resistivities of 10–20  $\Omega$  cm. The oxygen and carbon contents of the materials studied, as determined from infrared absorption measurements, are O,  $1.75 \times 10^{18}$   $\text{cm}^{-3}$  and C,  $1.9 \times 10^{16}$   $\text{cm}^{-3}$  for CZ Si and O,  $1.5 \times 10^{16}$   $\text{cm}^{-3}$  and C,  $1.4 \times 10^{15}$   $\text{cm}^{-3}$  for FZ Si. Two different erbium implants were performed: with ion energies of 320 keV (at room temperature) and 2 MeV (at 350 °C). The projected implant ranges are 112 and 560 nm, respectively, as inferred from profile simulation according to the “Transport of Ions in Matter” (TRIM) program.<sup>17</sup> The doses applied for the shallow implantation were  $1.9 \times 10^{12}$ ,  $3.2 \times 10^{12}$ , and  $4.5 \times 10^{12}$   $\text{cm}^{-2}$ , which correspond to Er peak concentrations of  $3 \times 10^{17}$ ,  $5 \times 10^{17}$ , and  $7 \times 10^{17}$   $\text{cm}^{-3}$ , respectively. For the 2 MeV implants, higher ion fluences of  $3 \times 10^{13}$  and  $8.7 \times 10^{13}$   $\text{cm}^{-2}$  (corresponding to peak concentrations of  $1.2 \times 10^{18}$  and  $3.5 \times 10^{18}$   $\text{cm}^{-3}$ ) were used. The samples showed no amorphization after implantation up to the highest dose investigated ( $3.2 \times 10^{13}$   $\text{cm}^{-2}$ ), as evidenced by x-ray diffraction studies. The samples were annealed at 900 °C in vacuum or in  $\text{N}_2$  ambient for 30 min. This procedure was reported to yield the maximum PL intensities CZ Si,<sup>3–5</sup> although for the FZ material annealing at 600 °C was found to be optimum.<sup>4</sup> Alternatively, for the 2-MeV-implanted samples a two-stage anneal (at 600 °C for 30 min with additional rapid thermal annealing at 900 °C for 15 s) was also performed. During the anneal, the samples were covered with Si wafers of the same type to prevent outdiffusion and contamination. Secondary-ion mass spectroscopy (SIMS) analysis reveals that in the 2-MeV-implanted samples the depth of the maximum implant concentration after anneal at 900 °C is in agreement with TRIM simulations; however, half of the implanted ions are incorporated in the tail of the profile extending about 3  $\mu\text{m}$  into the sample.

In order to investigate the possible formation of Er-dopant complexes and their influence on the PL yield, nitrogen and oxygen were coimplanted to peak concentrations varying from  $10^{16}$  to  $3.5 \times 10^{19}$   $\text{cm}^{-3}$ . The implantation energies were chosen so that the implant depths of the codopants and Er coincided.

Photoluminescence measurements have been performed with a Bomem DA 8.23 Fourier-transform spectrometer. The signal was detected with a cooled Ge or  $\text{In}_x\text{Ga}_{1-x}\text{As}$  detector, with resolutions down to 0.05  $\text{cm}^{-1}$ . The emission spectra shown in the figures were excited with the 514.5 nm Ar laser line. The samples were placed on a cold finger of a continuous-flow cryostat in vacuum. The excitation power density at the sample surface was typically less than 0.14  $\text{W}/\text{cm}^2$ . Substantial heating of the sample by the laser beam can be excluded, based on the measured position of the free excitonic gap, which is temperature dependent.

Deep-level transient spectroscopy measurements were carried out with use of a 1 MHz capacitance bridge, a pulse generator, and a liquid-nitrogen-cooled cryostat (77–400 K). The DLTS signal is obtained from the capacitance transients using a lock-in averaging method. The samples investigated were  $n$ -type Si with carrier concentrations of  $10^{16}$   $\text{cm}^{-3}$  and oxygen content of  $1.5 \times 10^{18}$   $\text{cm}^{-3}$ . Er was implanted at 640 keV with the dose of  $10^{12}$   $\text{cm}^{-2}$ , which corresponds to Er peak concentrations of  $8 \times 10^{16}$   $\text{cm}^{-3}$ . The samples were subjected to isochronal annealing steps (30 min) in the tem-

perature range of 200–1100 °C in nitrogen flow. The same annealing was performed on samples coimplanted with  $10^{13}$  cm<sup>-2</sup> oxygen ( $8 \times 10^{17}$  cm<sup>-3</sup>) at 95 keV. A set of samples was also annealed at 600 °C for 30 min and then isochronally (20 s) in the temperature range 700–1100 °C.

### III. DISTINCTION OF DIFFERENT CENTERS

The studies of the Si:Er system reported so far have been directed towards obtaining a higher luminescence yield together with a higher concentration of Er centers, and therefore they concentrated mostly on investigations of Er implanted into CZ material. In particular, because of the much lower PL intensities of Er-implanted FZ Si, no systematic comparison of the kind of light-emitting erbium centers active in CZ and FZ Si, when prepared under exactly the same conditions, has been done. Such measurements became possible by applying Fourier spectroscopy, which allows measurements of weak PL spectra at high resolution.<sup>14–16</sup>

Figure 1(a) shows the low-temperature (4.2 K) PL spectrum of a FZ Si sample implanted at 320 keV with the lowest of the applied ion doses ( $1.9 \times 10^{12}$  cm<sup>-2</sup>), corresponding to an Er peak concentration of  $3 \times 10^{17}$  cm<sup>-3</sup>. The sample was annealed at 900 °C for 30 min. The arrows labeled *C* indicate the positions of four of the five transitions related to an Er<sup>3+</sup> center with cubic site symmetry, observed by Tang *et al.*<sup>3</sup> The fifth line is close to the cutoff wavelength of the detector. Such a spectrum is commonly observed in Er-implanted CZ Si annealed at 900 °C for 30 min, especially for higher ion doses and higher implantation energies.<sup>4,5,10</sup>

Figure 1(b) depicts the spectrum of a CZ sample implanted and annealed in the same way as the sample in Fig. 1(a) and measured under exactly the same conditions. The same spectrum of cubic symmetry is observed at comparable intensity (lines labeled *C*). The main cubic line is not indicated as it is obscured by other, more intense PL lines visible in this region. The dominant emission in Fig. 1(b) originates, however, from a center with a close to axial symmetry. The energy positions of the seven transitions observed (from the eight expected for centers with lower than cubic symmetry) are indicated with dashed arrows. A closer inspection reveals splitting of these lines, showing that there are two very similar centers of that kind present, which will be discussed in the next section. These centers do not occur in FZ Si.

In Fig. 1(c) the PL spectrum of a CZ Si sample implanted at 2 MeV with a dose of  $3 \times 10^{13}$  cm<sup>-2</sup> (corresponding to an Er peak concentration of  $1.2 \times 10^{18}$  cm<sup>-3</sup>) is shown. The sample was also annealed at 900 °C. It can be seen that although the total PL intensity increases by a factor of 50, as compared to the spectrum shown in Fig. 1(b), the emission intensity of the cubic center increases by about two and a half orders of magnitude. In this sample even the fifth transition is visible. The main cubic line (positioned at 6504.8 cm<sup>-1</sup> at 4.2 K) is superimposed on two other PL lines (6504.1 and 6504.3 cm<sup>-1</sup>) of comparable intensity, which occur also in FZ and CZ Si for shallow implants. The PL of the axial centers dominant in Fig. 1(b), though still visible, is an order of magnitude less intense than that of the cubic centers.

The positions (in wave numbers) of the main Er PL lines observed in FZ and CZ Si for shallow and deep Er implants

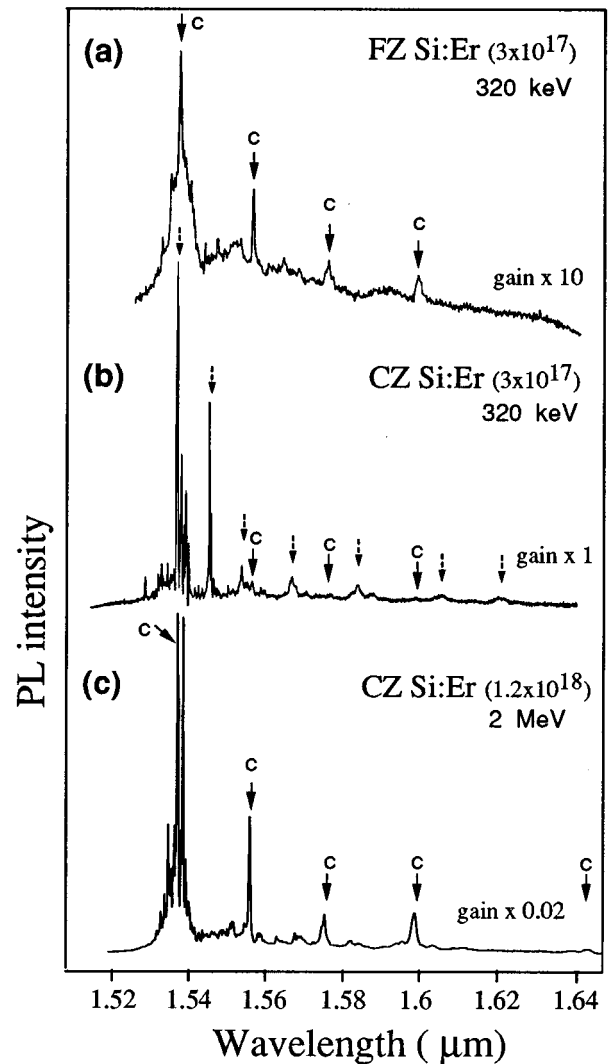


FIG. 1. PL spectra at 4.2 K of Er<sup>3+</sup> in FZ (a) and CZ Si (b) implanted with  $1.9 \times 10^{12}$  cm<sup>-2</sup> Er at 320 keV, as compared to CZ Si implanted with  $3 \times 10^{13}$  cm<sup>-2</sup> Er at 2 MeV (c). All samples were annealed at 900 °C for 30 min. The solid (labeled *C*) and dashed arrows indicate transitions related to Er centers with cubic and axial site symmetries, respectively.

after different annealing procedures are summarized in Table I. The transitions relating to the dominant emitting centers are emphasized with boldface type, whereas those with weaker intensity are marked by the use of italic type. All the line positions are given for a temperature of 4.2 K.

In order to study the effects of the Er concentration on the emission spectra, samples implanted with varying Er doses, but constant ion energy, were investigated. A moderate variation of the implant doses should ensure that no drastic change in the implantation-induced damage takes place. Figure 2 shows the short-wavelength range of the PL spectra measured in FZ (a) and CZ Si (b) with a resolution of 0.2 cm<sup>-1</sup>, for Er implanted at 320 keV to peak concentrations of  $3 \times 10^{17}$ ,  $5 \times 10^{17}$ , and  $7 \times 10^{17}$  cm<sup>-3</sup>. The chosen spectral range encompasses the two strongest features marked with dashed arrows in Fig. 1(b). The FZ Si spectra are magnified with respect to the CZ Si spectra by a factor of 5.

TABLE I. Wave numbers (in  $\text{cm}^{-1}$ ) of some of the characteristic PL lines observed in Er-implanted FZ and CZ Si, annealed at 900 °C for 30 min, or 600 °C for 30 min and 900 °C for 15 s. The line positions of the dominant emitting centers are emphasized with bold type and those with a weaker intensity with a *smaller font size*. The numbers are given with a tolerance of 0.2  $\text{cm}^{-1}$ .

FZ 320 keV 900 °C	CZ 320 keV 900 °C	CZ 2 MeV 900 °C	CZ 2 MeV 600+900 °C	Notation	FZ 320 keV 900 °C	CZ 320 keV 900 °C	CZ 2 MeV 900 °C	CZ 2 MeV 600+900 °C	Notation
			6570.9				6448.3	6448.3	
			6566.7			6447.0	6447.0	6447.0	
			6543.7				6446.5	6446.5	
	6542.4				6445.3		6445.3		
	6540.2		6540.2				6444.5		
			6536.1				6443.4		
			6534.6			6441.3	6441.3	<b>6441.3</b>	
6523.6						<b>6438.2</b>		6438.2	O2
6515.8	6515.8		6515.8			<b>6437.3</b>		6437.3	O1
6514.4	6514.4	6514.4				6436.5	6436.5		
			6514.0			6433.5	6433.5		
6511.6						6431.5	6431.5		
	6511.0	6511.0	6511.0					6430.7	
	<b>6508.6</b> <sup>a</sup>	6508.6 <sup>a</sup>	6508.6 <sup>a</sup>	O2	6429.7				
6508.1					6427.5				
	<b>6507.5</b> <sup>b</sup>	6507.5 <sup>b</sup>	6507.5 <sup>b</sup>	O1	<b>6426.0</b>	6426.0	<b>6426.0</b>	6426.0	C
6507.1					6421	6421		6421.9	
<b>6506.4</b>	6506.4					6417.6	6417.6	6417.6	
6505.8							6415		
6505.5	6505.5	6505.5	6505.5			6413.5		6413.5	
								6402.3	
<b>6504.8</b>	6504.8	<b>6504.8</b>	6504.8	C			6397.8		
6504.3	6504.3	<b>6504.3</b>	<b>6504.3</b>		6394				
6504.1	6504.1	<b>6504.1</b>	<b>6504.1</b>						
						<b>6386</b>		6386	O2
					6384	<b>6384.3</b>		6384.3	O1
6503.4	6503.4	<b>6503.4</b>				6379.6			
6502.8	6502.8				6379				
6502.5	6502.5	6502.5					6378.5	6378.5	
6500.8	6500.8	6500.8	6500.8				6375.5	6375.5	
6500.6	6500.6	6500.6	6500.6				6372		
6500.25	6500.25	6500.25					6368.5	6368.5	
6498.5	<b>6498.5</b>	<b>6498.5</b>	6498.5	ED1	6365				
6498.3	6498.3	6498.3	6498.3				6358.5	6358.5	
<b>6498.0</b>	6498.0	6498.0	6498.0		6350		6350	6350	
6497.5	6497.5	6497.5	6497.5		<b>6348</b>	6348	<b>6348</b>	6348	C
6496.2		6496.2	6496.2		6343	6343		6343	
	6495.3	6495.3	6495.3			6321	6321		
			6492.3				<b>6314.5</b>	6314.5	O1,O2
						6312	6312		
6490					6300	<b>6300</b>		6300	
6488.6		6488.6					6304		
	<b>6472.8</b> <sup>c</sup>	6472.8 <sup>c</sup>	6472.8 <sup>c</sup>	O1	6284		6286	6286	
6471.3	6471.3				<b>6256</b>	6256	<b>6256</b>	6256	C
	<b>6471</b> <sup>d</sup>	6471 <sup>d</sup>	6471 <sup>d</sup>	O2			6237		
	6468.7					<b>6229</b>		6229	O1,O2
6468.3			6468.3				6218		
	6467.8	6467.8						6169	
	6466.7	6466.7	6466.7			<b>6173</b>		6173	O1,O2
			<b>6464.4</b>			6155		6155	
							6100	6100	
							<b>6087</b>	6087	C

<sup>a</sup>The line consists of 6509.2, 6509.0, 6508.7, and 6508.5.

<sup>b</sup>The line consists of 6507.8 and 6507.45.

<sup>c</sup>The line consists of 6472.8 and 6472.6.

<sup>d</sup>The line consists of 6470.9 and 6471.2.

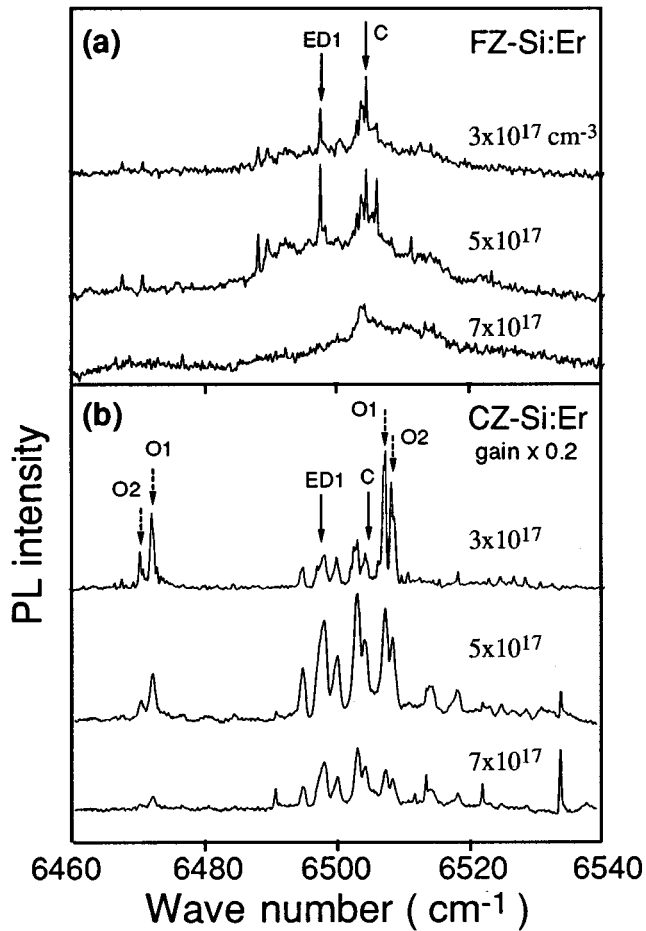


FIG. 2. High-energy range of the PL spectra in FZ (a) and CZ Si (b) for 320 keV Er implants. The peak concentrations (in  $\text{cm}^{-3}$ ) are indicated. The FZ Si spectra are magnified with respect to the CZ Si spectra by a factor of 5. The PL line positions of the cubic (C), axial symmetry (O1 and O2), and one of the low-symmetry (ED1) Er centers are indicated.

In FZ Si several quite intense PL lines are visible in the vicinity of the main cubic transition (at  $6504.8 \text{ cm}^{-1}$ , denoted with C), which are related to Er centers with lower site symmetry. The same emission lines occur also in CZ Si. They are, however, inhomogeneously broadened as compared to FZ material, because of an additional modification of the Er surroundings. In particular, the broad peak labeled C in CZ Si is composed of three almost equally intense PL lines at  $6504.1$ ,  $6504.3$ , and  $6504.8 \text{ cm}^{-1}$ , which are well resolved in FZ Si because of the narrower linewidths. The peak labelled ED1 is composed of four lines, all of which are also found in FZ Si, but the most intense line in CZ material is positioned at  $6498.5 \text{ cm}^{-1}$ , whereas in FZ Si the  $6498 \text{ cm}^{-1}$  line has the highest intensity. The PL intensities of the cubic and the low-symmetry lines increase upon increasing the Er concentration from  $3 \times 10^{17}$  to  $5 \times 10^{17} \text{ cm}^{-3}$  in both materials, and then they decrease again for a still higher erbium content. In contrast, the PL intensities of the axial symmetry centers, which occur only in CZ-grown material (denoted with O1 and O2 in Fig. 2), decrease monotonically with increasing Er concentration relative to the other (cubic and low-symmetry) lines observed.

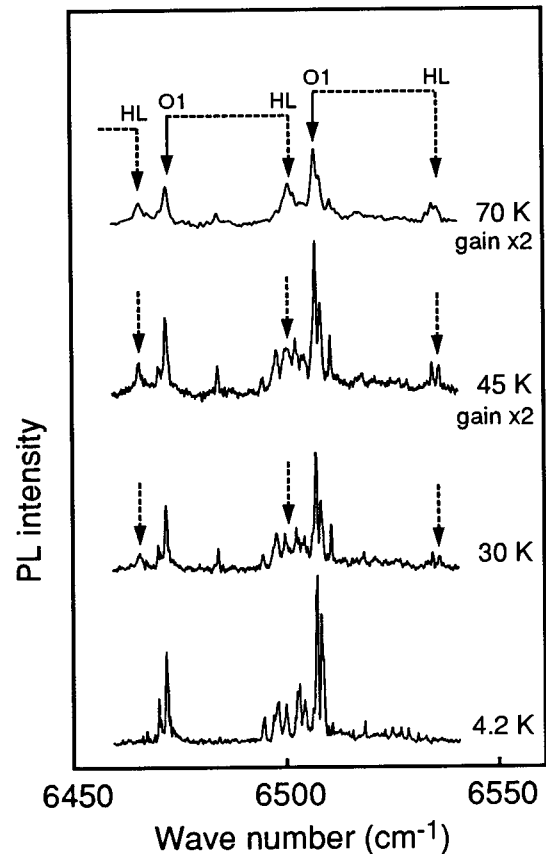


FIG. 3. Temperature evolution of the PL spectrum for the 320-keV-implanted CZ Si sample. The arrows mark the positions of the satellite lines (HL) associated with the Er-O1 lines, appearing at increased temperatures.

At elevated temperatures satellite lines to those of the Er-O1 center can be detected, as shown in Fig. 3. They are shifted by  $28.8 \text{ cm}^{-1}$  ( $3.57 \text{ meV}$ ) towards higher energies for each transition. Most likely, they originate from the next-lowest excited level of the crystal-field-split  $J=13/2$  multiplet and constitute an example of so-called “hot PL lines.” This assignment is confirmed by the characteristic temperature dependence. The PL intensity ratio  $I_{\text{HL}}/(I_0 + I_{\text{HL}})$ , where  $I_0$  and  $I_{\text{HL}}$  are the intensities of the main and the satellite lines, respectively, increases with increasing temperature with an activation energy equal to the energy distance between the two emission lines. Transitions from higher-lying excited levels can also be observed for the cubic PL spectrum although they appear at much higher temperatures. Figure 4 shows the PL spectrum of the sample with  $1.2 \times 10^{18} \text{ cm}^{-3}$  Er measured at 85 and 130 K, respectively. Two sets of satellite PL lines can be detected. One of them occurs from a state lying  $74.5 \text{ cm}^{-1}$  ( $9.2 \text{ meV}$ ) and another, weaker one from a state lying  $109 \text{ cm}^{-1}$  ( $13.5 \text{ meV}$ ) above the lowest excited state. The positions of the  $74.5 \text{ cm}^{-1}$  satellite lines associated with the second and third cubic transitions almost coincide with those of the first and second main transitions (the three main PL lines are split by  $78.3$  and  $78.5 \text{ cm}^{-1}$ , respectively) and can be separated only in high-resolution spectra. It can also be seen that at such temperatures the emission of all the lower-symmetry erbium centers, the intensity of which is comparable to that of the

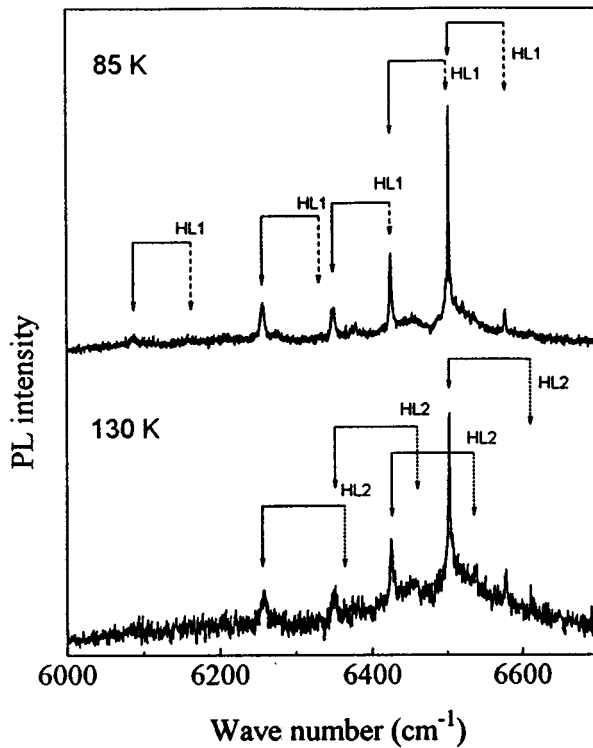


FIG. 4. PL spectra of the CZ Si sample implanted with  $3 \times 10^{13} \text{ cm}^{-2}$  Er at 2 MeV, measured at 85 and 130 K. Two sets of satellite lines associated with the cubic PL lines are visible and are denoted by HL1 and HL2. The positions of two of the HL1 lines cannot be separated from the main transitions for the energy scale used.

cubic spectrum at 4.2 K [see Fig. 1(c)], disappears. The energy level diagram of three Er centers is shown in Fig. 5.

Recently, two of the five lines assigned here to the crystal-field-split states of the cubic center were tentatively interpreted as phonon replicas of the dominant cubic PL line, whereas the hot line was ascribed to a transition from the  $n=1$  oscillator level of the excited electronic state.<sup>18</sup> Such an

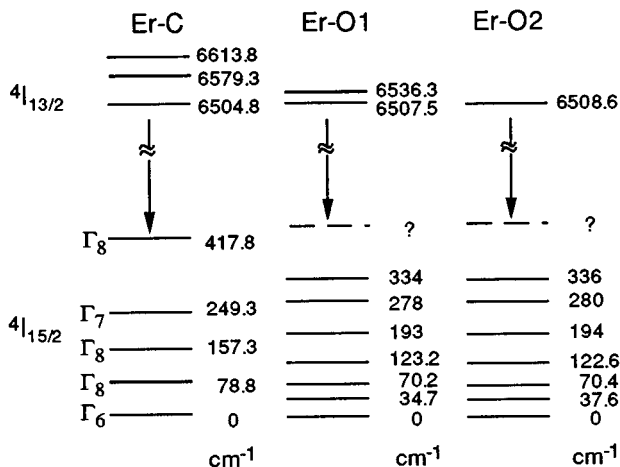


FIG. 5. Energy level diagram for the cubic (Er-C) and two lower symmetry (Er-O1 and Er-O2) erbium centers.

interpretation can be ruled out on the following grounds.

(i) If the hot lines were indeed connected with an “anti-Stokes” transition involving a local phonon, the higher-lying crystal-field states should interact with exactly the same phonon mode and with the same coupling strength, as every crystal-field transition is observed to exhibit a hot line with a similar intensity ratio to the main PL line. However, no “Stokes” phonon replicas are visible for the remaining cubic transitions, even though their intensity should be much bigger than that of the hot line.

(ii) Moreover, the intensity ratio of the PL lines ascribed in Ref. 18 to phonon replica, for the quoted Huang-Rhys factor of  $S=0.729$ , should change substantially when  $kT$  becomes comparable to the postulated local-mode energy,  $\hbar\omega=9.2 \text{ meV}$ , whereas all the five PL lines under discussion (labeled C in Table I) always retain the same relative intensities, irrespective of temperature (as seen in Fig. 4), as is characteristic for crystal-field-split transitions. Thus we conclude that the electron-phonon interaction for the  $4f$  states is negligible, as expected.

#### IV. MICROSCOPIC STRUCTURE OF CUBIC ER CENTERS

It is a well-known fact that rare-earth ions, when incorporated into ionic hosts (e.g., II-VI compounds or fluorites) in a nonisovalent +3 charge state, require charge compensation. Moreover, they tend to build complexes with charge-compensating impurities or lattice defects, which can act as efficient coactivators of the rare-earth intrashell luminescence. On these grounds it is often assumed that the high optical activity of Er implanted into CZ Si might be related to erbium forming complexes with oxygen, which is the highest-concentration contaminant of CZ Si (present at concentrations of about  $10^{18} \text{ cm}^{-3}$ ). A lack of such complexes in float-zone Si, where the oxygen content is lower by two orders of magnitude, is held responsible for the lower PL yield of Er-implanted FZ Si. This idea seemed to be supported by investigations of extended x-ray absorption fine structure (EXAFS),<sup>11</sup> which have shown that more than 80% of the Er ions incorporated into CZ Si are sixfold coordinated with oxygen ions, with a structure closely resembling that of  $\text{Er}_2\text{O}_3$ . Similar Er-O bond lengths and coordination values were also found in silica, in which the optical activity of Er is considered to be high.<sup>19</sup> In contrast, in FZ Si more than 85% of the Er ions were found to reside at sites almost identical with those of erbium in  $\text{ErSi}_2$ .<sup>11</sup> However, PL investigations of samples prepared in a similar way to those studied by EXAFS indicate that at best only 10% of the Er ions incorporated in CZ Si are optically active.<sup>9,10</sup> Moreover, the optically active Er ions occupy predominantly sites with well-defined cubic symmetry and the PL spectrum is very different from that observed for  $\text{Er}_2\text{O}_3$  (Ref. 9) or silica.<sup>20</sup> The observation of a well-resolved PL structure of Er in FZ Si, identical with that reported for the best-emitting CZ Si:Er samples,<sup>10</sup> sheds further doubts on the correlation between Er-O complex formation and the optical activity of erbium in silicon. It seems far more likely that it is the isolated Er center which is optically active rather than a highly symmetric, sixfold-coordinated Er-O complex.

As can be seen in Fig. 2 for low Er doses the PL intensi-

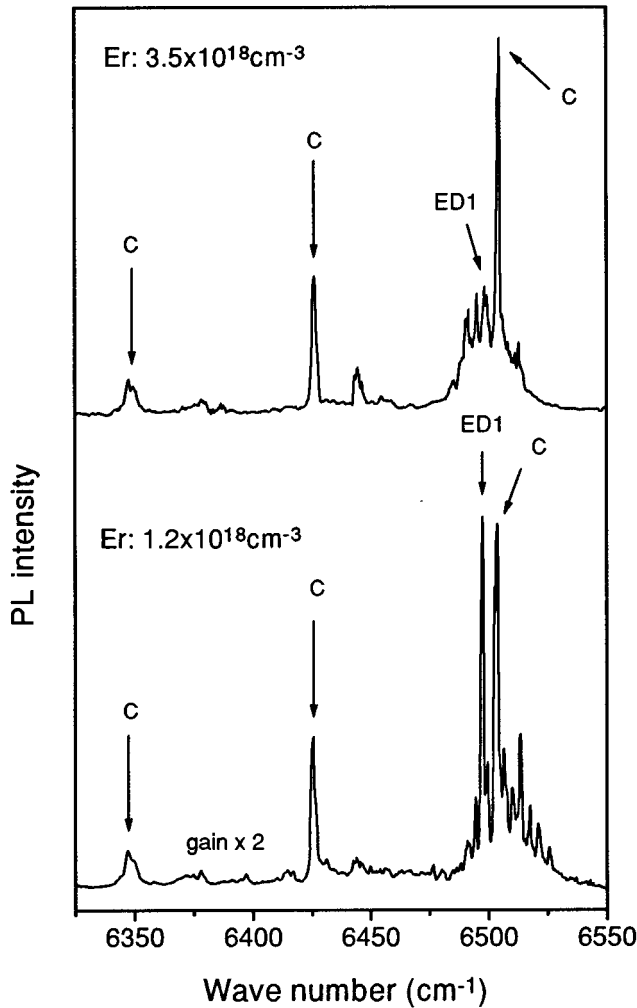


FIG. 6. PL spectra at 4.2 K of CZ Si implanted with  $3 \times 10^{13} \text{ cm}^{-2}$  Er at 2 MeV and annealed at  $900^\circ\text{C}$  for 30 min (lower and upper spectrum, respectively). The cubic transitions are labeled C; the PL line originating from a low-symmetry Er center, dominant after the heat treatment, is labeled ED1.

ties of the cubic center in CZ and FZ Si are similar, though the oxygen content of the latter material should not allow substantial formation of Er-O complexes. Moreover, when the dose is increased slightly, the PL intensity also increases in both materials, indicating that the center creation cannot be limited by the amount of oxygen present. Accidental thermal oxidation of the FZ sample during processing can be excluded since it should produce an amorphous  $\text{Er}_2\text{O}_3$  or  $\text{SiO}_2$  layer with characteristic, broadband Er PL spectra depending on whether Er was introduced before<sup>9</sup> or after oxidation.<sup>20</sup> Neither of the reported spectra occur in the investigated FZ Si samples. The broad background superimposed on the narrow-line PL spectrum of FZ Si:Er [visible in Fig. 1(a)] consists of an emission band at  $6500 \text{ cm}^{-1}$  and a weaker one at  $6460 \text{ cm}^{-1}$ . Both of them probably originate from Er clusters in the most heavily damaged region of the sample. The same bands are observed in Er-implanted CZ Si for much higher Er concentrations.

Figure 6 shows the evolution of the narrow PL lines related to low-symmetry Er centers into a broadband with increasing Er concentration for 2 MeV implants into the CZ Si

material (the samples were annealed at  $900^\circ\text{C}$  for 30 min). For the Er peak concentration of  $3.5 \times 10^{18} \text{ cm}^{-3}$  hardly any structure on the broadband is observed, but the main cubic PL line becomes stronger and noticeably narrower. The latter indicates that the cubic spectrum comes from a different region of the implanted layer. The higher-energy PL wing peaked at  $6512 \text{ cm}^{-1}$  ( $807.5 \text{ meV}$ ) in Fig. 6 originates from the so-called D1 dislocation line; the D2 line at  $7048 \text{ cm}^{-1}$  ( $874 \text{ meV}$ ) is also visible in wider-range spectra. The D1 and D2 emission lines are believed to be related to the presence of oxygen-induced stacking faults.<sup>21</sup> These two PL lines are present in all investigated CZ Si:Er samples heat treated at  $900^\circ\text{C}$ , and missing in the FZ material, which is a further indication that there is no noticeable increase of the oxygen content introduced during the processing of FZ samples.

Recently, a narrow-line cubic PL spectrum was reported at Er implanted into a silica layer obtained from a double-side oxidized silicon wafer.<sup>18</sup> This finding motivated us to investigate erbium emission in silica glass using high-resolution Fourier spectroscopy. To ensure that no Si inclusions remain in the material studied we implanted only  $10^{12}$  to  $10^{13} \text{ cm}^{-2}$  erbium (i.e., the same doping level as used by us in silicon) into a slice cut from a commercially available, high-purity silica-glass rod and annealed it in the same manner as the Si:Er samples. In samples so prepared, no Er emission was observed, either with 514.5 or 488 nm excitation. This is not surprising, since the direct excitation of Er, due to the low oscillator strength of intra- $4f$ -shell transitions, requires a much higher number of Er ions. Indeed, in bulk Er-doped silica the Er emission is easily detectable. Figure 7 shows the Er PL spectrum in  $\text{SiO}_2$  doped with  $1.6 \times 10^{19} \text{ cm}^{-3}$  Er (used as starting material for Er-doped fibers) as measured at 4.2 K with a resolution of  $0.5 \text{ cm}^{-1}$ . However, no narrow emission lines are observed. The spectrum consists of two very broad bands, positioned at energies about  $25 \text{ cm}^{-1}$  higher than those of the broad bands in Si:Er. In the same figure the PL emission of a CZ Si sample implanted with  $3.5 \times 10^{18} \text{ cm}^{-3}$  Er and  $3.5 \times 10^{19} \text{ cm}^{-3}$  oxygen, annealed at  $900^\circ\text{C}$ , is shown, as measured under the same experimental conditions (the relative numbers of Er ions accessible to the incident excitation in the Si and silica samples are  $1:10^5$ ). This emission is very different from the one measured in Si doped only with Er. No previously observed spectral line is visible and the peak positions of the dominant PL lines coincide with the positions of the silica bands. It appears reasonable to relate this spectrum to Er in  $\text{SiO}_2$  precipitates. However, since the spectral lines are extremely narrow (the linewidth is considerably smaller than that of Er in Si), the precipitates are presumably crystalline rather than glasslike. The above further supports the conclusion that the cubic PL spectrum in silicon originates from isolated Er ions and not from Er-O complexes.

The analysis of crystal-field splittings indicates that Er occupies an isolated, interstitial lattice site. The splittings of states belonging to a  $4f^n$  configuration with a definite total angular momentum  $J$  in a crystal-field potential of cubic point symmetry can be generally described by a perturbation of the form<sup>22</sup>

$$H = B_4(O_4^0 + 5O_4^4) + B_6(O_6^0 - 21O_6^4), \quad (1)$$

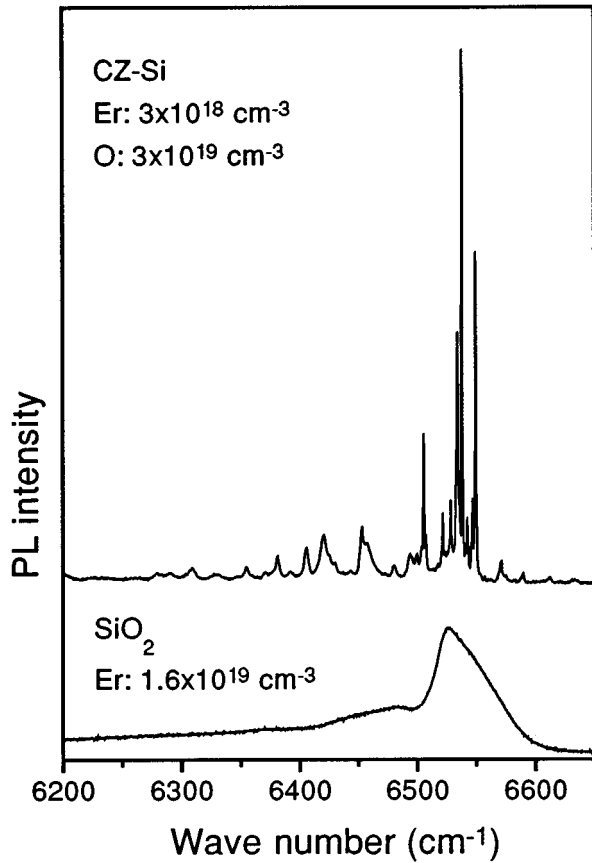


FIG. 7. Er PL spectra of volume-doped ( $1.6 \times 10^{19} \text{ cm}^{-3}$ ) silica fiber glass (lower spectrum) and CZ Si implanted with Er and oxygen (upper spectrum). The implant peak concentrations are indicated in the figure. Spectra were measured at 4.2 K with a resolution of  $0.5 \text{ cm}^{-1}$ .

where  $O_n^m$  are equivalent crystal-field operators expressed as functions of the components of  $J$ , whereas  $B_4$  and  $B_6$  are parameters which determine the scale of the splittings. In order to calculate the splittings of a given  $J$  multiplet for all possible values of the ratio between the fourth- and sixth-order terms, Lea, Leask, and Wolf<sup>22</sup> (LLW) have defined two parameters  $x$  and  $W$ , which relate to the crystal-field parameters  $B_4$  and  $B_6$  in the following way:

$$Wx = B_4 F(4), \quad W(1 - |x|) = B_6 F(6), \quad (2)$$

where  $F(4)$  and  $F(6)$  are factors introduced to keep the fourth- and sixth-order matrix elements in the same numerical range [for  $J = 15/2$ ,  $F(4) = 60$  and  $F(6) = 13\,860$ ]. In the LLW approach  $W$  is an energy scaling factor and the relative splittings are determined only by the value of  $x$ , which is a measure of the  $B_4/B_6$  ratio. The interval of  $-1 \leq x \leq 1$  spans the entire range of  $-\infty \leq B_4/B_6 \leq +\infty$ . Negative values of  $x$  correspond to tetrahedral coordination, whereas positive values occur for octahedral coordination.

Figure 8 shows the crystal-field splittings of the  $J = 15/2$  ground multiplet of  $\text{Er}^{3+}$  in a crystal field of cubic symmetry reproduced after LLW. The levels in Fig. 8 are labeled according to the convention for  $T_d$  symmetry. It can be seen that the experimentally observed pattern of lines cannot be

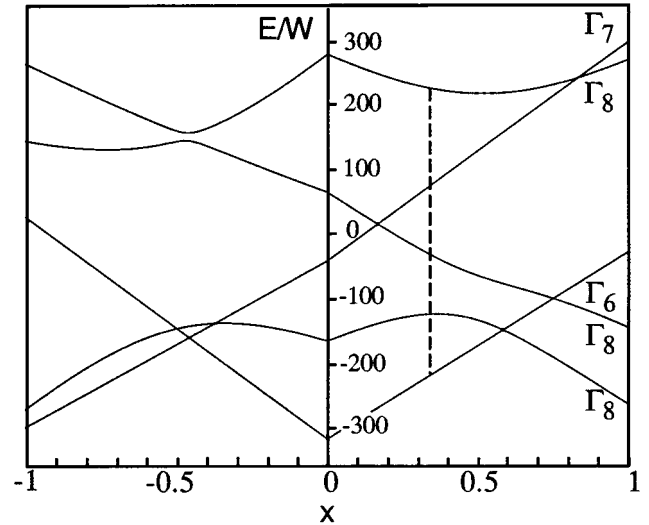


FIG. 8. Crystal-field splitting of the  $15/2$  multiplet of  $\text{Er}^{3+}$  after LLW (Ref. 22). The levels are labeled according to the convention for  $T_d$  symmetry.

obtained for a pure tetrahedral coordination ( $x < 0$ ); therefore Er cannot occupy a substitutional lattice site. The best fit to the experimental data was obtained for  $x = 0.35$  and  $W = 0.8864 \text{ cm}^{-1}$ . The positive sign of  $x$  indicates that erbium is incorporated in an interstitial  $T_d$  site, with four nearest neighbors and six close-lying next-nearest neighbors. This is in agreement with recent total-energy calculations, which predict that the tetrahedral interstitial site is the most stable configuration for  $\text{Er}^{3+}$  in silicon.<sup>23</sup>

## V. OXYGEN-RELATED CENTERS

The only Er centers which occur in the oxygen-rich CZ Si, but are not observed in FZ Si and therefore could be suspected of containing oxygen as part of the complex, are those labeled Er-O1 and Er-O2, visible in Figs. 1(b) and 2(b). These centers are observed in all investigated CZ Si samples but they dominate in the emission spectra only for low Er concentrations. As can be seen in Fig. 2(b), the PL intensity of these centers decreases with increasing Er dose relative to that of the cubic and other centers with lower site symmetry. Such behavior can be expected if the formation of the complex is limited by the number of available impurities. The pairing of erbium with intentional, shallow dopants, i.e., phosphorus and boron, can be immediately ruled out because the spectra are exactly the same in P- and B-doped samples. The only other residual impurity which could be considered a likely candidate to form complexes with Er is carbon, which is present in the investigated CZ Si wafers at a concentration of  $1.9 \times 10^{16} \text{ cm}^{-3}$  (as obtained from infrared absorption measurements). In order to check this possibility we implanted  $10^{17} \text{ cm}^{-3}$  Er into Si wafers with almost the same oxygen content ( $1.5 \times 10^{18} \text{ cm}^{-3}$ ) as the previously studied ones ( $1.75 \times 10^{18} \text{ cm}^{-3}$ ) but with an order of magnitude lower carbon concentration of  $3 \times 10^{15} \text{ cm}^{-3}$ . Since in this material the Er-O1 and Er-O2 centers also dominate the emission, it can be safely concluded that they are oxygen related.

The exact microscopic structure of the Er-O1 and Er-O2 complexes is so far unknown, but the energy level splittings are fairly well described by an axial crystal field. A careful inspection reveals that the first two O1 transitions have a structure consisting of two and the O2 of four lines with splittings of the order of  $0.2 \text{ cm}^{-1}$ , so that there could be altogether six slightly different complexes with a predominantly axial site symmetry. The PL line pattern (together with the relative intensities of the PL lines) is strikingly similar to that of the axial spectra observed in GaAs grown by metal-organic chemical-vapor deposition (MOCVD) in the presence of oxygen.<sup>24</sup> In the latter case also only seven of the eight transitions were detected. Moreover, it was shown that the center can be slightly modified by changing the second-nearest neighbor by AlAs alloying.<sup>24</sup>

It turns out that the concentration of the axial symmetry complexes depends on the oxygen content of the sample prior to Er implantation. Figure 9(a) depicts the high-energy range of the Er PL spectra in two CZ Si samples implanted with Er at 2 MeV to a peak concentration of  $1.2 \times 10^{18} \text{ cm}^{-3}$ . One of these samples was subsequently coimplanted with oxygen to an order of magnitude higher peak concentration. Both samples were then annealed at  $900 \text{ }^\circ\text{C}$  for 30 min. It can be seen in the oxygen-coimplanted sample (lower spectrum) that the PL intensity originating from centers with lower site symmetry increases relative to that of the cubic and axial ones. (In the depicted intensity scale only the PL lines related to the main Er-O transitions are visible.) Apparently, the main effect of such a codoping procedure is to produce more lattice damage. For even higher Er and O doses the implanted sample becomes amorphous, and after annealing at  $900 \text{ }^\circ\text{C}$  the typical Er PL disappears and a new spectrum with sharp emission lines positioned in the energy region coinciding with the PL bands of Er in silica is observed (see Fig. 7). To reduce the radiation damage connected with the coimplantation we annealed the heavily Er- ( $3.5 \times 10^{18} \text{ cm}^{-3}$ ) and O- ( $3.5 \times 10^{19} \text{ cm}^{-3}$ ) doped samples at  $600 \text{ }^\circ\text{C}$  for 30 min followed by an additional rapid thermal anneal at  $900 \text{ }^\circ\text{C}$  for 15 s. Such a two-step anneal is reported to ensure a good recrystallization of amorphous samples.<sup>25</sup> Indeed, in samples so prepared, no dislocation-related emission lines were observed. Also the intensity of the broad Er PL band, indicative of Er clustering, is strongly reduced as compared to the sample subjected to a  $900 \text{ }^\circ\text{C}$  heat treatment. The PL spectra of the Er-only- and (Er+O)-implanted samples are shown in Fig. 9(b). As can be seen, the PL is dominated by the emission of centers with low site symmetry, in contrast to the sample doped with the same Er dose but annealed at  $900 \text{ }^\circ\text{C}$  (compare also to Fig. 6), but at a lower maximum intensity.

The absolute PL intensity of the Er-O centers is, however, not very sensitive to the annealing procedure used. With oxygen coimplantation, again, the emission of high-symmetry centers (cubic and axial) disappears.

## VI. COMPLEXES WITH IMPLANTATION-INDUCED INTRINSIC DEFECTS

Beside the isolated, interstitial Er ions and O-related axial Er complexes there is a number of other Er centers present with lower site symmetry, as evidenced by the rich structure

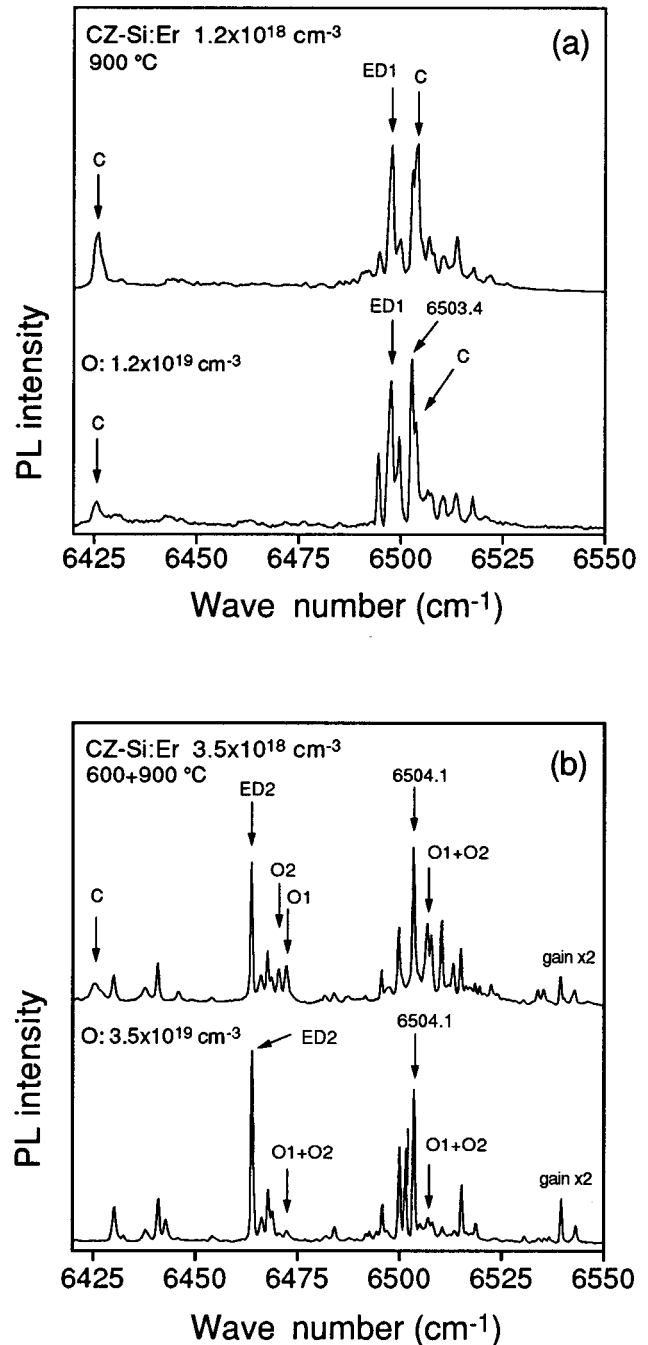


FIG. 9. (a) High-energy PL spectrum of CZ Si implanted with  $3 \times 10^{13} \text{ cm}^{-2}$  Er at 2 MeV as compared with the PL spectrum (below) in a sample coimplanted with  $3 \times 10^{14} \text{ cm}^{-2}$  O at 295 keV. Both samples were annealed at  $900 \text{ }^\circ\text{C}$  for 30 min. (b) PL spectra of Er-implanted ( $8.7 \times 10^{13} \text{ cm}^{-2}$ , 2 MeV) and O-coimplanted ( $8.7 \times 10^{14} \text{ cm}^{-2}$ , 295 keV) CZ Si annealed at  $600 \text{ }^\circ\text{C}$  for 30 min and  $900 \text{ }^\circ\text{C}$  for 15 s.

observed in the emission spectra in the vicinity of the main cubic transition at  $6504.8 \text{ cm}^{-1}$  (see Table I). Since there is little correlation among the relative intensities of the individual lines from sample to sample, it seems that most of the lines originate from slightly different sites. The intensities of these lines increase with increasing Er implant dose (for a constant implantation energy) relative to the cubic and axial

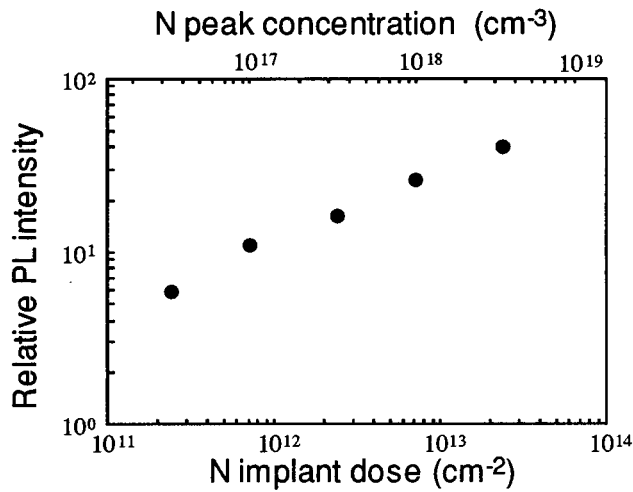


FIG. 10. PL intensity of the ED1 line normalized to the intensity of the main Er-O1 line as function of the N implant dose.

symmetry spectra (as shown in Fig. 2). The same effect is observed when the Er dose is kept constant but light ions, such as oxygen [see Fig. 9(a)], are additionally implanted at a matching implant depth. Coimplantation with nitrogen up to peak concentrations of  $10^{18} \text{ cm}^{-3}$  into CZ Si with Er (at 320 keV to the peak concentration of  $3 \times 10^{17} \text{ cm}^{-3}$ ) changes only the intensity of the various emission lines already present in the sample before nitrogen was added. For high N doses the ED1 line ( $6498.5 \text{ cm}^{-1}$ ) is the dominant PL line. The intensity ratio of ED1 to the main Er-O1 line is plotted vs N implant dose in Fig. 10. The same center is seen in CZ and FZ Si without N implantation. No new emission lines indicative of Er-N complex formation are visible. Therefore we relate the low-symmetry centers to the presence of implantation-induced lattice defects (such as silicon vacancies or vacancy complexes with residual silicon impurities) in the vicinity of the Er ion.

Since radiation defects are well known to introduce deep levels into the energy gap<sup>26</sup> we performed a systematic DLTS study of Er-implanted Si, looking for a correlation between the defect annealing behavior and the Er emission. In this series of experiments Er was implanted at 640 keV with a dose of  $10^{12} \text{ cm}^{-2}$  (corresponding to a peak concentration of  $8 \times 10^{16} \text{ cm}^{-3}$ , according to TRIM simulations). The material used was phosphorus doped, with an electron concentration of about  $10^{16} \text{ cm}^{-3}$ . The oxygen and carbon concentrations were  $1.5 \times 10^{18}$  and  $3 \times 10^{15} \text{ cm}^{-3}$ , respectively. One set of the implanted samples was annealed isochronally (30 min) in the temperature range of 200–1000 °C; another set was annealed at 600 °C for 30 min with an additional 20 s rapid thermal anneal (RTA) at temperatures varying between 700 and 1000 °C. Figure 11 depicts the sheet concentration of the different DLTS levels observed after a two-stage annealing procedure (vs RTA temperature) in samples implanted with Er only (a) as compared to samples coimplanted with oxygen (95 keV,  $10^{13} \text{ cm}^{-2}$ ) to a matching implant depth (b). The levels are indicated with different symbols with the corresponding apparent level enthalpies (in eV) given in parentheses. The defect concentrations in samples annealed for 30 min in the 700–1000 °C tempera-

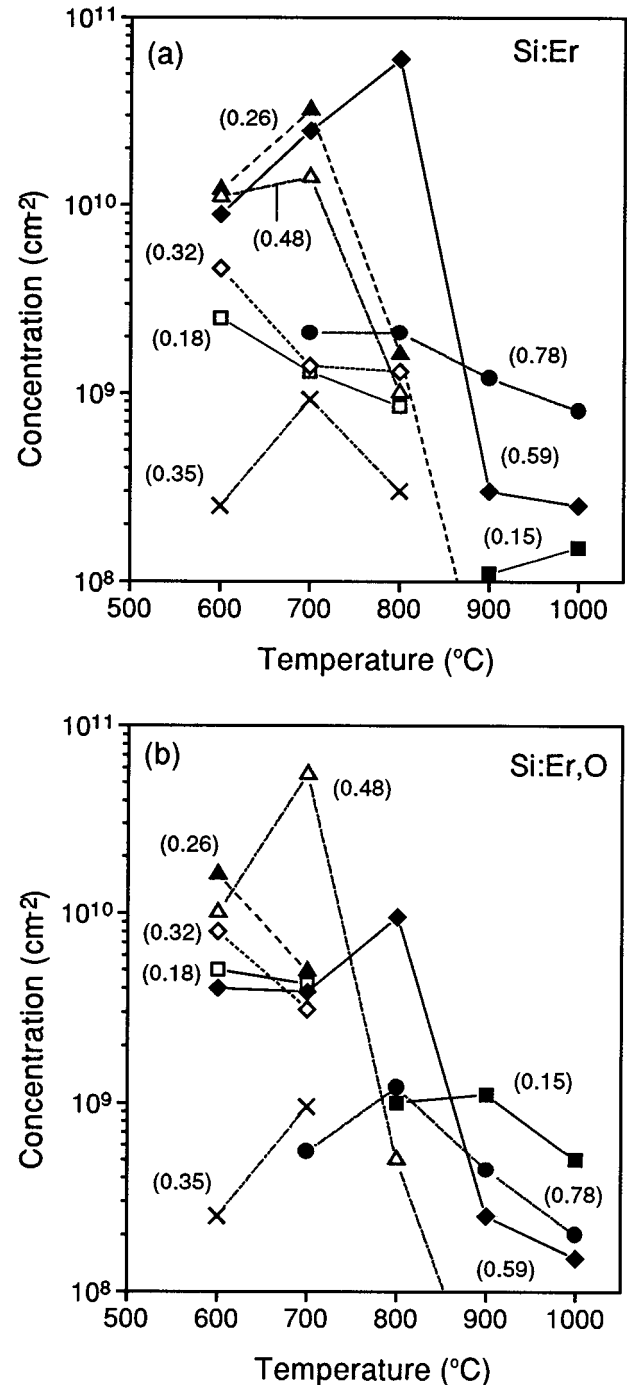


FIG. 11. Concentration of defects in *n*-type Si seen by DLTS vs RTA temperature (20 s). Samples were preannealed at 600 °C (30 min) and then given the RTA treatment: (a) after implantation of Er only ( $10^{12} \text{ cm}^{-2}$ , 640 keV); (b) coimplanted with  $\text{O}^+$  ( $10^{13} \text{ cm}^{-2}$ , 95 keV). The enthalpies of the DLTS levels, in eV units, are indicated in parentheses.

ture range are very similar to those shown in Fig. 11.

Though the Er dose is two orders of magnitude below the estimated amorphization threshold, the heavy Er ions cause displacement damage in Si in the form of defect clusters and isolated amorphous regions. Efficient annealing of vacancy- (*V*-) type defects, such as the O-*V* complex (0.17 eV) and the P-*V* pair (0.41 eV) was found to set in at about 600 °C;

only the divacancy level (0.21 eV) had disappeared already at 300 °C. The depth distribution of these defects coincides with the vacancy distribution according to TRIM profile simulations. A second group of defects is formed only after annealing at higher temperatures. The 0.48 eV and 0.59 eV levels appear already at 500 °C, the 0.35, 0.32, and 0.18 eV levels at 600 °C, and the deepest 0.78 eV level at 700 °C, whereas the 0.15 eV level is visible only above 800 °C. Some of the levels were already reported in Si:Er,<sup>6</sup> but have not been observed in Si implanted with other ions. The depth distribution profiles of those defects agree with that of the erbium implant. Obviously, they are formed during annealing from dissociation products of radiation defects and Er ions. At elevated temperatures there is a competition between generation and dissociation of such Er-defect complexes, and their concentrations start to decrease. Most of them disappear after annealing at 900 °C; however, the defects with the emission enthalpies of 0.78, 0.59, and 0.15 eV remain stable up to 1100 °C. In samples coimplanted with oxygen, a significant reduction of the concentrations of the deeper defects is observed, in particular after annealing above 800 °C. Evidently, in the presence of oxygen the deeper levels are passivated. Simultaneously, the concentration of the 0.15 eV level is found to increase, implying that the latter defect is oxygen related.

The existence of deep electron trap levels can obviously affect both the Er emission and the near-band-edge luminescence of Si. The relative changes of the PL intensities of the various Er centers as a function of the annealing temperature are given in Fig. 12. For comparison, the intensity of the TO-phonon-assisted phosphorus-bound exciton (P-BE) PL line is shown. The luminescence was measured at 4.2 K on the same samples used in the DLTS experiments and reported in Fig. 11(a). Unfortunately, the emission intensity cannot be directly related to the concentration of the emitting center, as it depends also on the excitation efficiency and radiative recombination probability as well as on the competition of various radiative and nonradiative recombination channels. Hence only a qualitative analysis of the observed trends will be presented.

Comparing the optical and the DLTS results, it becomes evident that the deep levels are efficient carrier recombination centers, as the P-BE luminescence intensity (denoted with solid squares) increases by a factor of 2.5 for the annealing temperature of 900 °C, for which most of the defects disappear, and the concentration of the 0.59 eV level is strongly reduced. At higher annealing temperatures, the exciton PL intensity decreases again, which is an indication that other recombination centers are formed (shallow centers or possibly hole trap defects) which are not detected in the present DLTS study. The integrated Er emission intensity (indicated with open squares in Fig. 12) follows the annealing curve of the P-BE PL. However, the annealing behavior of the individual Er centers is very different. After a 700 °C anneal, the cubic center (labeled *C*) dominates the PL spectra, but the PL intensity decreases rapidly for higher annealing temperatures. This can be understood in terms of a transformation of isolated Er centers into different types of complexes. The intensities of PL lines related to low-symmetry Er centers (the integrated intensity of all the low-symmetry centers observed after annealing at 700 °C is indicated with

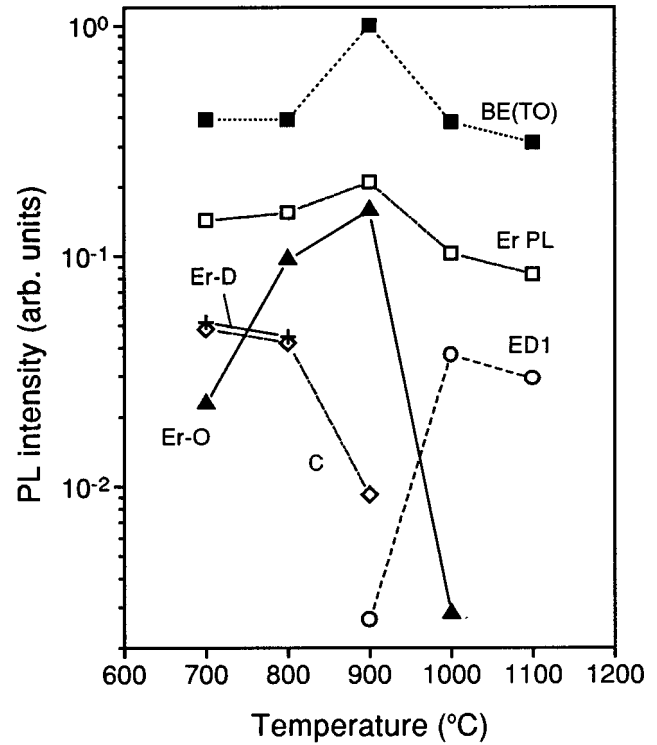


FIG. 12. PL intensity of various Er emitting centers observed in *n*-type Si vs RTA temperature (20 s). Samples were preannealed at 600 °C (30 min) and then given the RTA treatment. The intensity of the TO-phonon-assisted P-BE is indicated with solid squares and the integrated Er PL with open squares. The centers are labeled as follows: *C*, cubic center (diamonds); Er-O, axial symmetry complexes (triangles); Er-*D*, various low-symmetry centers not observed after a 900 °C anneal (crosses); ED1, one of the typical low-symmetry centers dominant for high Er doses (circles). The Er dose was  $10^{12}$  cm<sup>-2</sup> at 640 keV. The corresponding DLTS level concentrations are shown in Fig. 11.

crosses) are also found to decrease with increasing annealing temperature, because the relevant Er-defect complexes dissociate. Such centers are not observed after annealing at 900 °C. In contrast, the emission intensity of the axial symmetry Er-O complexes (labeled O1+O2) is found to increase for RTA temperatures up to 900 °C. This increase is most likely due to the annealing of nonradiative carrier recombination centers (the near-band-edge PL reaches a maximum at the same annealing temperature as the Er-O centers), as well as to the decreasing concentrations of cubic and defect-related Er centers, which otherwise compete in the excitation transfer from the host to Er, rather than to a temperature-induced generation of the center. Above 900 °C the intensity of the Er-O emission is strongly reduced and the emission of a number of new low-symmetry Er centers is observed, among them the center labeled ED1, which was found earlier to dominate the PL of heavily nitrogen-coimplanted samples even after 900 °C annealing. The same optically active Er centers, with very similar annealing curves, are observed in samples codoped with oxygen. The only noticeable difference is that the host emission intensity does not decrease for annealing temperatures above 900 °C, which can be related to oxygen gettering of carrier recombination centers.

In summary, we have found that the low-symmetry PL centers observed after heat treatment up to 800 °C exhibit a similar annealing behavior as some of the energy levels observed in DLTS. However, for annealing temperatures in the range 900–1000 °C no correlation between the light-emitting Er centers and the DLTS defect concentrations was noticed. In particular, the oxygen-related 0.15 eV level is not connected with any of the optically active Er centers detected. It seems that the electrically active Er complexes are not necessarily optically active.

The results discussed so far clearly demonstrate that the formation of Er-O complexes cannot be held responsible for the orders of magnitude higher Er PL yield observed in CZ Si as compared to FZ Si implanted and annealed at exactly the same conditions (Fig. 1). A much more plausible explanation is that oxygen in CZ Si passivated carrier recombination centers, thus increasing the carrier lifetime and the efficiency of Er excitation. This assumption is supported by the fact that not only the Er emission but also the host emission observed in Er-implanted FZ Si is very weak. We have examined the phonon-assisted free exciton (FE) and phosphorus-bound exciton (P-BE) PL as measured in FZ and CZ Si implanted with the same Er dose (at 320 keV) and annealed at 900 °C for 1/2 h. All experimental conditions were also kept constant. It turns out that the intensity ratio of the near-band-gap emissions of CZ and FZ Si reflects exactly the Er PL intensity ratio in those materials. This proves that the low Er PL yield of FZ Si is related to the lower excitation efficiency rather than to the lower number of optically active Er centers. Apparently, in oxygen-poor FZ Si the implantation defects alone act as gettering centers for fast-diffusing lifetime killers, such as Fe and Cu, which are attracted to the damage region during annealing. Our experiments have shown that the host emission of Er-implanted but not annealed FZ Si is more than two orders of magnitude higher than after annealing. This process would also explain the much faster degradation of the FZ Si:Er emission with increasing Er concentration (see Fig. 2) as compared to CZ Si:Er.

## VII. EXCITATION MECHANISM

One of the main hindrances as far as the application of rare-earth- (RE-) activated materials for light-emitting diodes is concerned is the low probability of  $4f-4f$  transitions and hence the low excitation and radiative deexcitation rates. Possible RE excitation via coherent or incoherent energy transfer from recombining electron-hole pairs is also not expected to be extremely efficient.<sup>27</sup> A much higher PL yield is expected for such rare-earth ions, which can localize free carriers forming bound excitons (BE's), since, e.g., core polarization induced by the externally bound carriers may lead to the admixture of higher-lying core states and thus to the relaxation of the selection rules. Once such a state is formed, the nonradiative decay of the RE-BE with energy transfer to the RE core states (so-called impurity Auger recombination) is the most likely recombination path, provided that the BE recombination energy is higher than the core excitation energy and the energy mismatch is not too great. In the latter case, both radiative BE recombination and RE intrashell emission can be observed [as, e.g., for Yb<sup>3+</sup> in ZnS (Ref.

28)], which is then an unambiguous proof of the existence of the RE-BE state. In most cases, however, the formation of a RE-BE as an intermediate step in the RE excitation process can be concluded only indirectly, by studying the PL excitation or by the observation of a characteristic temperature dependence of the PL intensity [as, e.g., for Er<sup>3+</sup> in GaAs (Ref. 29)]. Recently, direct radiative recombination of the RE-BE was also observed for Yb- and Er-activated InP.<sup>30–32</sup>

By analogy, we may expect that the erbium excitation in Si may also involve the formation of an Er-bound exciton, especially as the existence of a trap level related to an interstitial Er<sup>3+</sup> impurity in Si (which is necessary for exciton binding) has been predicted theoretically.<sup>23</sup> So far, however, the arguments are based on speculations.<sup>7,33</sup> The first experimental evidence that Er excitation indeed proceeds via energy transfer from Er-bound excitons comes from the observed temperature dependence of the Er PL, shown in Fig. 13. In the low-temperature region (up to about 50 K, depending on the sample) the quenching of the PL intensity ( $I$ ) is found to be described by the formula

$$I(T) = I(0)[1 + C_1 \exp(-E_1/kT)]^{-1}, \quad (3)$$

which is characteristic of a thermally deactivated excitation process. The PL deactivation energies ( $E_1$ ) determined for the various Er centers range from 5 to 15 meV, and depend only on the kind of emitting center but not on the sample studied. These energy values are of the order of typical impurity-BE binding energies in Si.<sup>34</sup> It seems that the low-temperature PL intensity of Er centers is governed by the efficiency of exciton capture and detachment and by the energy transfer efficiencies. The exciton binding energies and the coupling constants  $C_1$  for some of the investigated Er centers are summarized in Table II. It can be seen that the coupling coefficients differ considerably for the various Er centers and can change by an order of magnitude from sample to sample.

The meaning of the coupling constant can be illustrated in a very simple manner. Let us consider a specific Er center, with a total concentration  $N$ , which can trap free excitons forming a BE state. The number of such bound excitons  $N_{BE}$  depends on the number of excitons available for capture,  $n_{FE}$ , as well as on the capture  $c_{BE}$  and thermal emission  $e_{BE}$  coefficients of the center:

$$\frac{d}{dt} N_{BE} = n_{FE} c_{BE} (N - N_{BE} - N^*) - N_{BE} e_{BE} \exp(-E_{BE}/kT). \quad (4)$$

$N^*$  is the number of excited Er ions, after the excitation is transferred from the BE to Er core states.  $N^*$  depends on the transfer rate  $\beta$  as well as on the lifetime  $\tau$  of the excited state:

$$\frac{d}{dt} N^* = \beta N_{BE} - N^*/\tau. \quad (5)$$

Hence the luminescence intensity, which depends on the steady-state value of  $N^*$ , takes the form

$$I(T) = I(0) \left( 1 + \frac{e_{BE}}{n_{FE} c_{BE} (1 + \beta\tau)} \exp(-E_{BE}/kT) \right)^{-1}, \quad (6)$$

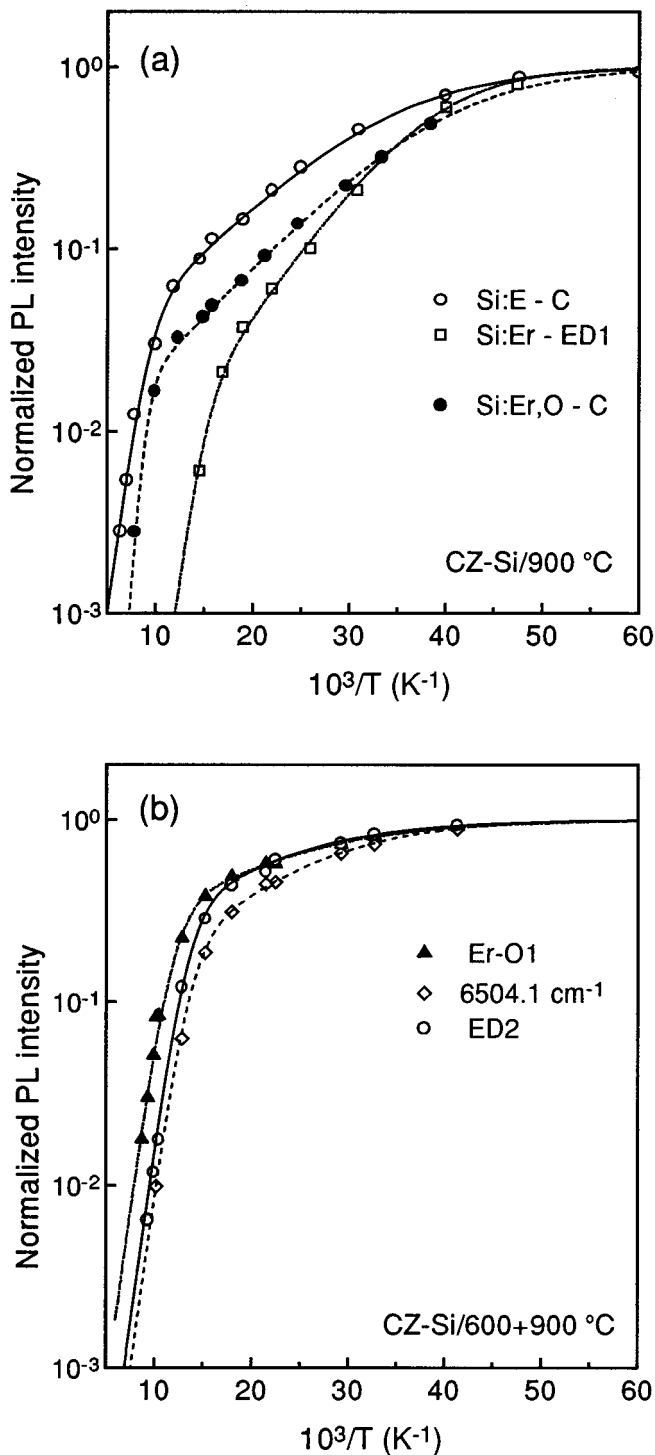


FIG. 13. (a) Arrhenius plot of the PL intensity of the cubic (open circles) and ED1 (open squares) Er centers in *p*-type CZ Si implanted with  $3 \times 10^{13} \text{ cm}^{-2}$  Er as compared to the PL quenching of the cubic center (solid circles) in *p*-type CZ Si implanted with Er (2 MeV,  $8.7 \times 10^{13} \text{ cm}^{-2}$ ) and oxygen (285 keV,  $8.7 \times 10^{13} \text{ cm}^{-2}$ ). The samples were annealed at 900 °C for 30 min. (b) Arrhenius plot of the PL intensity of the dominant emitting centers observed in Er-implanted (2 MeV,  $8.7 \times 10^{13} \text{ cm}^{-2}$ ) *p*-type CZ Si annealed at 600 °C for 30 min and 900 °C for 15 s. The lines drawn in (a) and (b) are fitted with the formula and parameters given in Table II.

which has the same form as Eq. (3).

Since the number of excitons available for capture under steady-state pumping conditions depends strongly on the concentrations and capture cross sections of competing trap centers, the preexponential factor can vary by orders of magnitude from one sample to another. The variation of the prefactor for different Er centers in the same sample, however, reflects mainly the difference in the exciton trapping and/or energy transfer efficiencies of the centers themselves. The simple model presented above does not allow the actual capture cross sections or energy transfer rates of the investigated centers to be determined (in particular, the temperature dependence of the coupling constants has been neglected); however, some conclusions about their relative PL efficiencies can be drawn. A comparison of the parameter values summarized in Table II indicates, e.g., that in samples annealed at 900 °C the cubic center is more efficient than the low-symmetry center ED1, despite the bigger exciton binding energy of the latter.

Intrashell excitation of a RE ion due to Auger-type energy transfer from recombining RE-BE's is expected to be a particularly efficient RE excitation channel. The efficiency of such an excitation path for the Er impurity in Si is demonstrated in Fig. 14, which shows the temperature evolution of the PL intensities of four different Er centers, measured in a *P*-doped CZ Si sample, implanted with  $3.2 \times 10^{12} \text{ cm}^{-2}$  Er at 320 keV. For such implantation energies the Er-doped layer lies close to the sample surface (100 nm) and most of the incident photons are absorbed in an Er-free region of the sample. The generated free excitons then diffuse over macroscopic distances and can be captured by native trap centers before reaching the Er layer, which limits the Er excitation at low temperatures. At elevated temperatures excitons can be thermally released from the trap centers and the probability of Er excitation should increase. Such an increase is in fact observed for three of the investigated centers, with the main lines positioned at  $6498.5 \text{ cm}^{-1}$  (squares),  $6500.2 \text{ cm}^{-1}$  (diamonds), and  $6511 \text{ cm}^{-1}$  (dots). The PL intensity for these centers reaches a maximum only at about 15 K. The increase can be fitted (lines drawn in Fig. 14) with an activation energy of 5 meV, which is the binding energy of the phosphorus-BE observed in this sample. For the Er-O1 complex (denoted with triangles) no increase is observed, which indicates that exciton capture at that center is particularly efficient.

The excitation mechanism involving Er-bound excitons turns out to be the dominant one even at 70 K. This is demonstrated in the time-resolved Fourier spectroscopy experiment reported previously<sup>35</sup> and later on also in Ref. 36. The time evolution of the PL intensity after a 30  $\mu\text{s}$  excitation pulse at 70 K shows that after termination of the pump pulse the Er PL intensity increases substantially for about 200  $\mu\text{s}$  (reaching twice the initial value) before it starts to decay. At such long times after the pump is turned off, no free or shallow-impurity-bound excitons are expected. In fact, the near-band-gap emission, which in the sample studied was of comparable intensity to the Er emission at temperatures around 10 K, was found to disappear already at 50 K. It is therefore evident that the increase of the Er PL intensity by a factor of 2 is solely due to energy transfer from the recombining Er-BE's.

TABLE II. PL deactivation energies and coupling constants obtained for various Er centers from the fit of experimental data with the formula  $I(T) = I(0)[1 + C_1 \exp(-E_1/kT) + C_2 \exp(-E_2/kT)]^{-1}$ . The accuracy of the determined energies is limited by the systematic error connected with temperature measurements. The maximum error for the coupling constants is less than 20%.

Implant energy (keV), dose (cm <sup>-2</sup> )	Anneal temp. (°C)	Main line position (cm <sup>-1</sup> )	Center label	$E_1$ (meV)	$C_1$	$E_2$ (meV)	$C_2$
Er: 320, 3.2×10 <sup>12</sup>	900	6507.5	O1	9.0±0.5	10		
		6498.5	ED1	14.0±0.5	90		
		6500.2		5.4±0.5	8		
		6511.0		5.2±0.5	11		
Er: 2000, 3×10 <sup>13</sup>	900	6504.8	C	10.0±0.5	55	80±8	6×10 <sup>4</sup>
		6498.5	ED1	15.0±0.5	740	80±8	6×10 <sup>7</sup>
Er: 2000, 8.7×10 <sup>13</sup>	900	6504.8	C	11.0±0.5	160	150±10	3×10 <sup>8</sup>
O: 285, 8.7×10 <sup>13</sup>							
Er: 2000, 8.7×10 <sup>13</sup>	600+900	6507.5	O1	8.7±0.5	6.5	78±8	1.2×10 <sup>5</sup>
		6504.8	C	10.0±0.5	18.8	78±8	6×10 <sup>5</sup>
		6464.4	ED2	9.9±0.5	9	78±8	5×10 <sup>5</sup>
		6504.1		10.5±0.5	18	78±8	9×10 <sup>5</sup>

### III. Er PL QUENCHING AT ELEVATED TEMPERATURES

The thermal ionization of Er-bound excitons with their subsequent recombination on competing traps is, however, not the mechanism responsible for near-room-temperature quenching of the Er PL. At temperatures above 100 K a second deactivation process becomes visible. In contrast to the Er-BE ionization process, the thermal deactivation energy for the high-temperature quenching does not depend on the emitting center.

Figure 13(a) depicts the temperature dependence of the normalized PL intensity for the interstitial cubic Er center (open circles) and the ED1 center (squares) as measured in *p*-type CZ Si implanted with 3×10<sup>13</sup> cm<sup>-2</sup> Er at 2 MeV and annealed at 900 °C for 30 min. This dependence shows two distinct quenching processes: Er-BE thermalization with energies of about 10 meV for the cubic center and 15 meV for the ED1 center, and a second process governed by the deactivation energy of about 80 meV, which occurs for both centers. Fits to the data with the formula  $I = [1 + C_1 \exp(-E_1/kT) + C_2 \exp(-E_2/kT)]^{-1}$  are shown by the lines drawn for the following parameters:  $C_1 = 55$ ,  $C_2 = 6.0 \times 10^4$  for the cubic center and  $C_1 = 740$ ,  $C_2 = 6.5 \times 10^7$  for the ED1 center. As can be concluded from the values of the coupling constants, the 80 meV deexcitation process is responsible for the actual vanishing of the Er emission at increased temperatures in the sample studied. The same deactivation energy is observed for all the optically active Er centers observed in exactly the same material implanted with 8.7×10<sup>13</sup> cm<sup>-2</sup> Er at 2 MeV, but annealed with the two-stage process (600 °C for 30 min with 15 s RTA at 900 °C). Apparently, the energy is also independent of the annealing procedure applied. The temperature dependencies of the PL intensity for the axial Er-O1 center and two lower-symmetry complexes are shown in Fig. 13(b). The fitting parameters for the various centers observed (together with the cubic center not shown in the figure) are given in

Table II. Surprisingly, a different deactivation energy, about 150 meV, appears when the sample is codoped with oxygen. The temperature dependence of the cubic PL intensity in the O-coimplanted sample is shown in Fig. 13(a).

The mechanism responsible for the Er PL quenching in the high-temperature regime is, so far, not clear. The existence of a well-defined, but sample-dependent, deactivation energy suggests that the process might involve some trap center. We expect that at elevated temperatures this center is ionized and Er can recombine nonradiatively due to Auger-type energy transfer to the thermally released free carriers. Such a deexcitation process is one of the dominant nonradiative recombination channels for rare-earth impurities in semiconductors.<sup>37</sup> We observe a substantial decrease of the Er lifetime with increasing temperature, which is in agreement with the proposed interpretation. It turns out, moreover, that even at 4.2 K the Er recombination is not entirely radiative, as the lifetime was found to decrease by about 7% upon a very moderate increase of the pump power (from 20 to 100 mW). This suggests that even the light-induced carrier population at low temperatures can influence the nonradiative decay rate. The very high coupling constants (10<sup>5</sup>–10<sup>8</sup>) observed for the PL quenching in the high-temperature regime, as evidenced in Table II, reflect not only the effectiveness of the nonradiative Er recombination channel but also the decreasing efficiency of excitation transfer from the host to Er. In this regime the free excitons are thermally dissociated, which increases the probability of nonradiative carrier recombination on other defect centers in the sample. This effect seems to depend on radiation damage, i.e., for the same cubic center the coupling constant increases by about an order of magnitude for a three times higher Er dose, and by an additional two orders of magnitude when oxygen is coimplanted.

We observe no experimental indication of nonradiative Er recombination related to energy transfer back to the Er-bound exciton, which was suggested to limit the high-

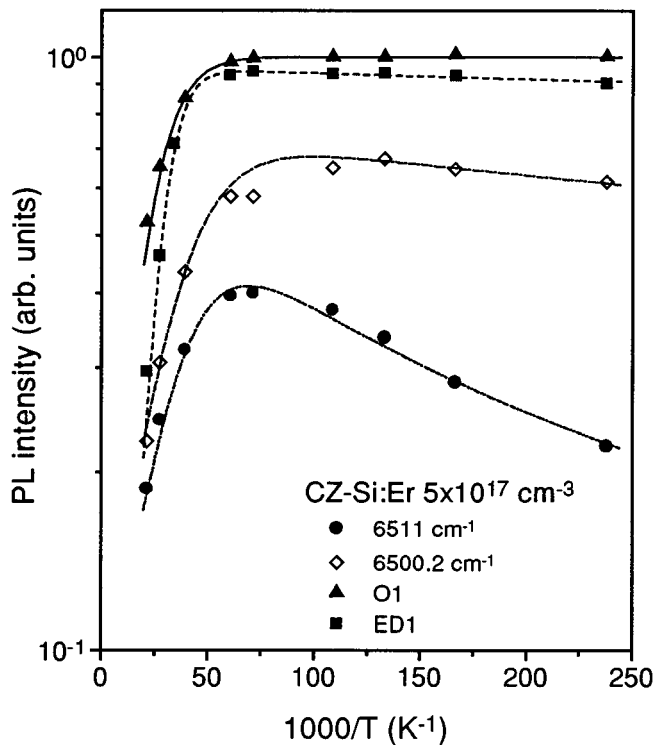


FIG. 14. Temperature dependence of the PL intensity of axial Er-O1 (triangles) and lower-symmetry Er centers in *n*-type CZ Si implanted with  $3.2 \times 10^{12} \text{ cm}^{-2}$  Er at 320 keV. The lines drawn are calculated with the fitting parameters (for the PL quenching) given in Table II. The low-temperature rise in PL intensity is fitted with an activation energy of 5 meV.

temperature PL yield of Er in silicon.<sup>10</sup> In such a mechanism the thermal PL deactivation energy should depend on the energy mismatch between the BE and Er recombination energies, in other words, it should depend only on the kind of emitting center and not on the sample. In contrast to that, we observe a change of the PL deactivation energy from 80 to 150 meV for the same center after oxygen coimplantation. The suppression of the 80-meV-activated PL quenching is a further indication that oxygen passivates carrier trap centers. The 150 meV deactivation energy observed in oxygen-codoped samples is probably connected with an O-related trap center, rather than with the energy required for the acti-

vation of the back-transfer process. It seems that in Er-implanted Si non radiative recombination due to the presence of radiation-damage-related centers by far dominates over the back-transfer process.

## IX. CONCLUSIONS

We have observed a number of erbium centers with different crystal surroundings: (i) isolated Er ions at interstitial sites, observed after annealing at 900 °C, independent of the material studied (FZ or CZ Si); (ii) Er-oxygen complexes with nearly axial site symmetry, which occur only in oxygen-rich CZ Si but at limited concentrations; (iii) various Er complexes with residual radiation defects, the concentration of which increases with increasing Er implant dose or with light-ion (N,O) coimplantation. Some of the Er-defect complexes remain stable up to unusually high annealing temperatures (1100 °C). The formation of axial Er-O centers is not very efficient and probably takes place already during implantation, as it is only slightly affected by varying the annealing conditions. Thus the lower PL yield of Er-implanted FZ Si as compared to CZ Si is related to oxygen gettering of nonradiative recombination centers rather than Er-O complexes.

We have shown that the Er intrashell luminescence is predominantly excited via energy transfer from Er-bound excitons and that the exciton binding energies are slightly different for different Er centers. The efficiency of the temperature quenching of Er PL is also center dependent; however, the thermal release of bound excitons is not the main deexcitation mechanism. Of all the investigated Er centers, the cubic and axial oxygen-related ones show the highest PL yield at high temperatures.

## ACKNOWLEDGMENTS

We are indebted to A. Polman, K. Takahei, A. Taguchi, T. Gregorkiewicz, and C. A. J. Ammerlaan for very helpful discussions. It is a pleasure to thank H. Ruckser, J. Enzenhofer, and M. Bruckner, who participated in some of the measurements presented. One of us (H.P.) acknowledges support from the Bundesministerium für Wissenschaft und Forschung, Vienna, during her stay in Linz. This work was supported by the Gesellschaft für Mikroelektronik, Vienna and Polish Research Council, Grant No. 8 S501 029 05.

<sup>1</sup>H. Ennen, J. Schneider, G. Pomrenke, and A. Axmann, *Appl. Phys. Lett.* **43**, 943 (1983).

<sup>2</sup>H. Ennen, G. Pomrenke, A. Axmann, K. Eisele, W. Haydl, and J. Schneider, *Appl. Phys. Lett.* **46**, 381 (1985).

<sup>3</sup>Y. S. Tang, K. C. Heasman, W. P. Gillin, and B. J. Sealy, *Appl. Phys. Lett.* **55**, 432 (1989).

<sup>4</sup>J. Michel, J. L. Benton, R. F. Ferrante, D. C. Jacobson, D. J. Eaglesham, E. A. Fitzgerald, Y. H. Xie, J. M. Poate, and L. C. Kimerling, *J. Appl. Phys.* **70**, 2672 (1991).

<sup>5</sup>J. Michel, L. C. Kimerling, J. L. Benton, D. J. Eaglesham, E. A. Fitzgerald, D. C. Jacobson, J. M. Poate, Y. H. Xie, and R. F. Ferrante, *Mater. Sci. Forum* **83-87**, 653 (1992).

<sup>6</sup>J. L. Benton, J. Michel, L. C. Kimerling, D. C. Jacobson, Y.-H. Xie, D. J. Eaglesham, E. A. Fitzgerald, and J. M. Poate, *J. Appl. Phys.* **70**, 2667 (1991).

<sup>7</sup>S. Coffa, F. Priolo, G. Franzo, V. Bellani, A. Carnera, and C. Spinella, *Phys. Rev. B* **48**, 11 782 (1993).

<sup>8</sup>S. Coffa, G. Franzo, F. Priolo, A. Polman, and R. Serna, *Phys. Rev. B* **49**, 16 313 (1994).

<sup>9</sup>F. Y. G. Ren, J. Michel, Q. Sun-Paduan, B. Zheng, H. Kitagawa, D. C. Jacobson, J. M. Poate, and L. C. Kimerling, in *Rare Earth Doped Semiconductors*, edited by G. S. Pomrenke, P. B. Klein, and D. W. Langer, MRS Symposia Proceedings No. 301 (Materials Research Society, Pittsburgh, 1993), p. 87.

- <sup>10</sup>J. Michel, F. Y. G. Ren, B. Zheng, D. C. Jacobson, J. M. Poate, and L. C. Kimerling, *Mater. Sci. Forum* **143-147**, 707 (1994).
- <sup>11</sup>D. L. Adler, D. C. Jacobson, D. J. Eaglesham, M. A. Marcus, J. L. Benton, J. M. Poate, and P. H. Citrin, *Appl. Phys. Lett.* **61**, 2181 (1992).
- <sup>12</sup>D. J. Eaglesham, J. Michel, E. A. Fitzgerald, D. C. Jacobson, J. M. Poate, J. L. Benton, A. Polman, Y. H. Xie, and L. C. Kimerling, *Appl. Phys. Lett.* **48**, 2797 (1991).
- <sup>13</sup>G. Franzo, F. Priolo, S. Coffa, A. Polman, and A. Carnera, *Appl. Phys. Lett.* **64**, 2235 (1994).
- <sup>14</sup>H. Przybylinska, J. Enzenhofer, G. Hendorfer, M. Schoisswohl, L. Palmethofer, and W. Jantsch, *Mater. Sci. Forum* **143-147**, 714 (1994).
- <sup>15</sup>H. Przybylinska, G. Hendorfer, M. Bruckner, L. Palmethofer, and W. Jantsch, *Appl. Phys. Lett.* **66**, 490 (1995).
- <sup>16</sup>W. Jantsch, G. Hendorfer, M. Bruckner, L. Palmethofer, and H. Przybylinska, in *Proceedings of the XXII International Conference on the Physics of Semiconductors*, edited by D. J. Lockwood (World Scientific, Singapore, 1995), p. 2411.
- <sup>17</sup>J. F. Ziegler, J. P. Biersack, and U. Littmark, *The Stopping and Range of Ions in Solids* (Pergamon, New York, 1985), Vol. 1.
- <sup>18</sup>I. de Maat-Gersdorf, T. Gregorkiewicz, C. A. J. Ammerlaan, and N. A. Sobolev, *Semicond. Sci. Technol.* **10**, 666 (1995).
- <sup>19</sup>M. A. Marcus and A. Polman, *J. Non-Cryst. Solids* **136**, 260 (1991).
- <sup>20</sup>A. Polman and J. M. Poate, *J. Appl. Phys.* **73**, 1669 (1993).
- <sup>21</sup>A. R. Peaker, B. Hamilton, G. R. Lahiji, and G. Lorimer, *Mater. Sci. Eng. B* **4**, 123 (1989).
- <sup>22</sup>K. R. Lea, M. J. M. Leask, and W. P. Wolf, *J. Phys. Chem. Solids* **23**, 1381 (1962).
- <sup>23</sup>M. Needels, M. Schlüter, and M. Lannoo, *Phys. Rev. B* **47**, 15 533 (1993).
- <sup>24</sup>K. Takahei, A. Taguchi, Y. Horikoshi, and J. Nakata, *J. Appl. Phys.* **76**, 4332 (1994).
- <sup>25</sup>F. Priolo, S. Coffa, G. Franzo, C. Spinella, A. Carnera, and V. Bellani, *J. Appl. Phys.* **74**, 4936 (1993).
- <sup>26</sup>G. Watkins, in *Deep Centers in Semiconductors*, edited by S. T. Pantelides (Gordon and Breach, New York, 1986), p. 164.
- <sup>27</sup>S. Schmitt-Rink, C. M. Varma, and A. F. J. Levi, *Phys. Rev. Lett.* **66**, 2782 (1991).
- <sup>28</sup>H. Przybylinska, K. Swiatek, A. Stapor, A. Suchocki, and M. Godlewski, *Phys. Rev. B* **40**, 1748 (1989).
- <sup>29</sup>J. E. Colon, D. W. Elsaesser, Y. K. Yen, R. L. Hengehold, and G. S. Pomrenke, *Mater. Sci. Forum* **83-87**, 671 (1992).
- <sup>30</sup>B. J. Heijmink Liesert, M. Godlewski, A. Stapor, T. Gregorkiewicz, C. A. J. Ammerlaan, J. Weber, M. Moser, and F. Scholz, *Appl. Phys. Lett.* **58**, 2237 (1991).
- <sup>31</sup>K. Thonke, K. Pressel, G. Bohnert, A. Stapor, J. Weber, M. Moser, A. Malassioti, A. Hangleiter, and F. Scholz, *Semicond. Sci. Technol.* **5**, 1124 (1990).
- <sup>32</sup>B. Lambert, A. Le Corre, Y. Toudic, C. Lhomer, G. Grandpierre, and M. Gauneau, *J. Phys. Condens. Matter* **2**, 479 (1990).
- <sup>33</sup>H. Efeoglu, J. H. Evans, T. E. Jackman, B. Hamilton, D. C. Houghton, J. M. Langer, A. R. Peaker, D. Perovic, I. Poole, N. Ravel, P. Hemment, and C. W. Chan, *Semicond. Sci. Technol.* **8**, 236 (1993).
- <sup>34</sup>*Semiconductors. Physics of Group IV Elements and III-V Compounds*, edited by O. Madelung, Landolt-Börnstein, New Series, Group III, Vol. 17, Pt. a (Springer, Berlin, 1982), p. 56.
- <sup>35</sup>H. Przybylinska, G. Hendorfer, M. Bruckner, W. Jantsch, and L. Palmethofer, in *Proceedings of the 2nd International Conference on f-Elements*, Helsinki, 1994 [*J. Alloys Compounds* **225**, 555 (1995)].
- <sup>36</sup>Jung H. Shin, G. N. van den Hoven, and A. Polman, *Appl. Phys. Lett.* **67**, 377 (1995).
- <sup>37</sup>J. M. Langer, in *Electroluminescence*, edited by S. Shionoya and H. Kobayashi, Springer Proceedings in Physics Vol. 38 (Springer, Berlin, 1989), pp. 16–23.